

Diffusion-Guided Gaussian Splatting for Large-Scale Unconstrained 3D Reconstruction and Novel View Synthesis

Niluthpol Chowdhury Mithun^{1*}, Tuan Pham^{2*}, Qiao Wang¹, Ben Southall¹, Kshitij Minhas¹, Bogdan Matei¹, Stephan Mandt², Supun Samarasekera¹, Rakesh Kumar¹

¹SRI International, Princeton, NJ, USA
¹firstname.lastname@sri.com

²University of California, Irvine, CA, USA
²{tuan.pham; mandt}@uci.edu

Abstract

Recent advancements in 3D Gaussian Splatting (3DGS) and Neural Radiance Fields (NeRF) have achieved impressive results in real-time 3D reconstruction and novel view synthesis. However, these methods struggle in large-scale, unconstrained environments where sparse and uneven input coverage, transient occlusions, appearance variability, and inconsistent camera settings lead to degraded quality. We propose GS-Diff, a novel 3DGS framework guided by a multi-view diffusion model to address these limitations. By generating pseudo-observations conditioned on multi-view inputs, our method transforms under-constrained 3D reconstruction problems into well-posed ones, enabling robust optimization even with sparse data. GS-Diff further integrates several enhancements, including appearance embedding, monocular depth priors, dynamic object modeling, anisotropy regularization, and advanced rasterization techniques, to tackle geometric and photometric challenges in real-world settings. Experiments on four benchmarks demonstrate that GS-Diff consistently outperforms state-of-the-art baselines by significant margins.

1. Introduction

Recent progress 3DGS and NeRFs have revolutionized real-time 3D reconstruction and view synthesis, particularly under controlled conditions with dense inputs [10, 18]. However, these methods falter in unconstrained environments where sparse data, transient occlusions, appearance variability, varying camera models, and image acquisition issues introduce significant artifacts and quality degradation. While recent works have sought to address specific challenges with tailored modules [3, 13, 24], most methods remain optimized for small-scale benchmarks, limiting their generalization to unconstrained real-world scenarios.

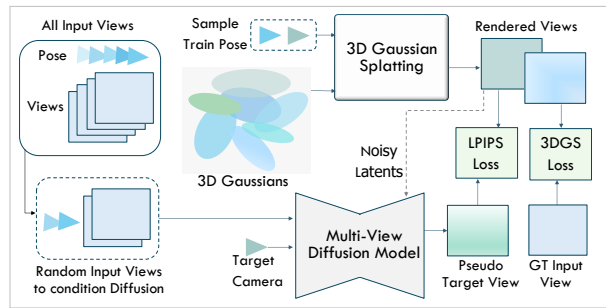


Figure 1. Brief Illustration of the Proposed GS-Diff Approach.

In such environments, sparse and uneven input coverage creates an under-determined reconstruction problem, leading to incomplete geometry and subpar rendering. To address this, we introduce GS-Diff, a novel adaptation of the 3DGS framework guided by prior knowledge from multi-view diffusion model (Fig. 1). GS-Diff synthesizes pseudo-observations conditioned on input images using the diffusion model, which provides supplementary viewpoints for 3DGS optimization, effectively converting the 3D reconstruction problem into a more constrained setting. These synthesized views enhance the optimization pipeline, significantly improving reconstruction fidelity and novel view synthesis under sparse and inconsistent conditions.

To further address the challenges unique to unconstrained in-the-wild scenarios, GS-Diff incorporates several enhancements into the 3DGS framework. These include monocular depth priors for improved geometric constraints, appearance embeddings to account for illumination variability, dynamic object modeling to address transient occlusions, anisotropy regularization to prevent over-elongated Gaussians, and advanced rasterization techniques such as mip-filtering and absolute gradients to reduce aliasing and blurring. Together, these adaptations make GS-Diff robust to real-world complexities.

Experiments on diverse datasets [1, 2, 20, 21], including ULTRRA benchmark, demonstrate GS-Diff achieves significant improvements over existing methods, bridging the

*Equal Contribution

gap between controlled benchmarks and real-world applications for scalable, high-fidelity 3D scene reconstruction.

2. Related Works

3D Gaussian Splatting for unconstrained scenes: 3DGS-based methods have recently demonstrated significant advancements in 3D scene reconstruction, particularly in controlled benchmarks [10, 11, 16]. Several recent works have improved vanilla 3DGS method to tackle specific challenges in 3D reconstruction, such as improving rendering quality and fine-grained details [27, 28, 30, 31], addressing sparse-view reconstruction [6, 24, 34], handling lighting variations [5, 13], transient occlusions [13, 26], and mitigating camera artifacts [19]. These methods have broadened the applicability of 3DGS in structured scenarios with prior knowledge of scene characteristics. Regression-based generalizable 3DGS methods have also emerged, that directly predict 3D representations from a small number of input images using feed-forward models [3, 4, 25]. These approaches bypass time-consuming optimization steps, but they often focus mainly on sparse-view cases and fail to produce high-quality view synthesis when exposed to out-of-distribution inputs. However, in real-world, unconstrained scenes, we frequently lack any prior knowledge of the environment or the types of challenges that might arise. It compounds the difficulty of applying current methods effectively, as they are often ill-equipped to handle unexpected complexities or variations in these settings.

Multi-View Diffusion for Novel View Synthesis: Recent advancements in diffusion models have highlighted their potential for synthesizing novel views, particularly in scenarios with sparse datasets. Multi-view diffusion models such as EscherNet [12], Cat3D [7], and ViewCrafter [29] have shown decent results in generating plausible views from limited reference images. These models leverage powerful generative priors to extrapolate missing details and enhance visual coherence, offering an alternative to traditional neural rendering pipelines. Despite their promise, these models are typically constrained to small spatial regions with limited reference images, making them prone to hallucinations in complex scenes. Moreover, their outputs often lack strict 3D consistency, posing challenges for direct integration into reconstruction pipelines. While few recent efforts have explored ways to integrate diffusion models within reconstruction frameworks [7, 15, 22], challenges remain in achieving 3D consistency, scaling to large scenes, and generalizing to diverse real-world conditions.

3. Proposed Approach

3.1. 3D Gaussian Splatting Baseline

3D Gaussian Splatting: 3DGS [10] represents a scene as trainable 3D Gaussians, each defined by a center $\mu \in \mathbb{R}^3$,

covariance matrix Σ , opacity α , and spherical harmonic (SH) coefficients for view-dependent color c . These Gaussians are projected onto the image plane [35], yielding 2D Gaussians with transformed means and covariances. A tile-based rasterizer sorts the Gaussians by depth and computes final pixel colors \hat{C} using α -blending:

$$\hat{C} = \sum_{i=1}^n c_i \alpha_i \prod_{j=1}^{i-1} (1 - \alpha_j) \quad (1)$$

where c_i is SH-based color and α_i is the opacity-weighted contribution of the i -th splatted Gaussian. With a given set of images with known poses, training optimizes SSIM and L_1 losses between predicted image \hat{I} and ground truth I :

$$\mathcal{L}_{\text{GS}} = \lambda_{\text{ssim}} \cdot \text{SSIM}(\hat{I}, I) + (1 - \lambda_{\text{ssim}}) \cdot \|\hat{I} - I\|_1 \quad (2)$$

During training, Gaussians with low opacity or large size are pruned, while those with high gradients are split or cloned heuristically to improve 3D representation.

Scaffold-GS: 3DGS’s heuristic splitting and cloning often leads to Gaussian drift and redundancy. Scaffold-GS [16] addresses this by organizing 3D Gaussians around anchor points derived from Structure-from-Motion (SfM). Each anchor is linked to a feature vector encoding local scene structure and generates k neural Gaussians with positions $\mu_i = x_v + O_i \cdot l_v$, where x_v is anchor position, O_i are predicted offsets and l_v is a scaling factor.

Neural Gaussian properties like opacity, scale, rotation, and color are decoded from anchor features via multi-layer perceptrons (MLPs). For instance, opacity α_i is computed as $\alpha_i = F_\alpha(\hat{f}_v, \Delta v_c, \vec{d}_{v_c})$, using an MLP F_α , anchor feature \hat{f}_v , viewing distance Δv_c , and camera direction \vec{d}_{v_c} .

During densification, new anchors are added where Gaussian gradients are high, and low-transparency anchors are pruned, improving robustness and storage efficiency compared to vanilla 3DGS. We adopt Scaffold-GS as our base 3D reconstruction pipeline.

3.2. Incorporating Diffusion Priors

3D reconstruction with limited inputs in unconstrained scenes often leads to overfitting or degraded performance at novel viewpoints. To address this, we integrate prior knowledge in the GS training via a diffusion model (trained for multi-view consistent view synthesis) (Fig. 1).

Multi-View Diffusion Prior in 3DGS Training: The Multi-View (MV) Diffusion model predicts scene appearance from novel viewpoints while maintaining consistency with given posed images. Pre-trained on public multi-view datasets, the model regularizes 3DGS by generating augmented pseudo-training views conditioned on nearby views. An additional loss aligns diffusion-augmented views with corresponding 3DGS-rendered views. Generating all the

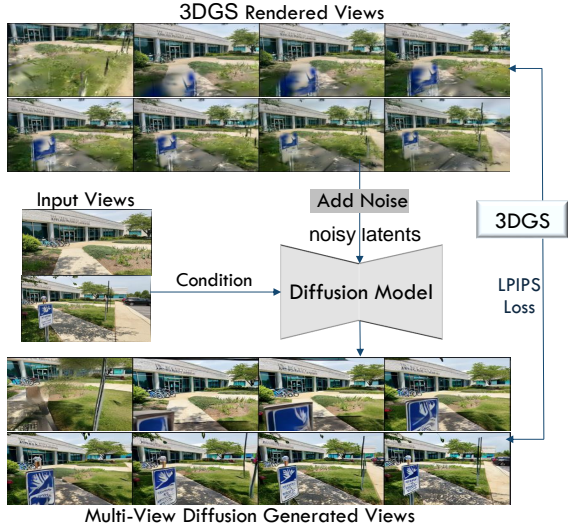


Figure 2. Iterative workflow of the integrated diffusion process with the proposed GS-Diff pipeline.

augmented views one time makes the model prone to hallucinations and 3D inconsistencies of the diffusion model. In this regard, we develop an integrated framework that applies diffusion-based view augmentation iteratively at every N^{th} step during the 3DGS training (Fig. 2).

Training pairs with proximal camera poses are selected, and a spline interpolation generates intermediate camera trajectories. Target augmented cameras sample new views, where noisy 3DGS-rendered latents are input to the MV Diffusion model. The diffusion model denoises these inputs into high-quality generated images (I_i^D), and compared to 3DGS-rendered views (\hat{I}_i) using LPIPS loss [22,33]. LPIPS prioritizes high-level semantic similarity while potentially overlooking low-level inconsistencies, making it suitable for ours. We define LPIPS-based loss as:

$$L_{GS}^D = \mathbb{1} \left(L_{LPIPS}(\hat{I}_i, I_i^D) \leq \epsilon \right) \cdot L_{LPIPS}(\hat{I}_i, I_i^D) \quad (3)$$

It excludes rendered-generated pairs with LPIPS exceeding ϵ (e.g., $\epsilon = 0.5$) from optimization to ensure stable training.

Diffusion Model Training: EscherNet serves as our baseline diffusion model [12]. EscherNet leverages a pre-trained 2D diffusion model (Stable Diffusion), and augments it with a camera positional encoding to handle arbitrary numbers of reference and target views. Its lightweight view encoding and scene-agnostic design, which avoids volumetric operations or ground-truth geometry, make it both efficient and adaptable to incorporate in our pipeline.

To align EscherNet effectively with the requirements of efficient 3DGS optimization, we introduce two key modifications in training: (1) training on lower-resolution images with fewer intermediate views to reduce computational overhead, and (2) employing a noise schedule shift towards higher noise levels, similar to [7]. These adaptations en-

Table 1. DreamSim Comparison on ULTRRA and WRIVA Sets.

Dataset (no. images)	ULTRRA		WRIVA-AIDI				WRIVA-MTA	
	ID-1901 (96)	CM-2601 (77)	S05 (25)	S06 (15)	S07 (10)	S08 (5)	S01 (50)	S02 (50)
Dev.-Baseline	0.088	0.319	0.59	0.82	0.57	0.90	0.53	0.78
Vanilla-3DGS	0.127	0.165	0.32	0.38	0.42	0.62	0.39	0.45
Scaffold-GS	0.102	0.135	0.25	0.34	0.39	0.54	0.37	0.40
Ours GS-only	<u>0.064</u>	<u>0.102</u>	<u>0.20</u>	<u>0.26</u>	<u>0.33</u>	<u>0.48</u>	<u>0.32</u>	<u>0.35</u>
Ours	0.058	0.087	0.19	0.21	0.26	0.39	0.28	0.33

able EscherNet to complement 3DGS effectively, particularly under challenging real-world conditions.

3.3. Adapting Base GS to Unconstrained Scenes

We also integrate several enhancements to our base GS pipeline to address challenges in modeling unconstrained scenes, focusing on color representation, depth modeling, dynamic objects, appearance variability, and efficiency.

Softmax-Depth Loss with Monocular Depth Priors: To improve geometric reconstruction, we introduce a scale-invariant depth loss \mathcal{L}_{sD} guided by monocular depth priors (Marigold [9]). Instead of alpha-blending, we use softmax-scaled depth rendering [24], which emphasizes depth gradients by weighting depth values with Gaussian opacities, prioritizing solid objects and reducing floating artifacts.

Appearance Embedding for Lighting Variability: We adopt global appearance embedding [17], to compensate for appearance and lighting variability in input images. Each training image is assigned a learnable embedding vector, which helps adapt the GS model to in-the-wild scenes.

Dynamic Object Handling with Masks: To mitigate the impact of dynamic objects, we use binary masks (indicating selected objects) generated using a semantic segmentation model. This mask \mathcal{M} is then used to multiply the per-pixel loss defined in Eq.1 and the training loss effectively ignores the dynamic object regions.

Rasterization Improvements: We incorporate two recent improvements to the 3DGS Rasterizer. First, absolute pixel gradients [28,31] replace directional gradients to better differentiate well-reconstructed regions. Second, Mip-Splatting [30] mitigates aliasing artifacts by using a 2D low-pass Mip filter, replacing the screen-space dilation filter.

Opacity and Scaling Regularization: We also apply regularization [23] to opacity and scaling to encourage fewer Gaussians, improving the efficiency of 3D representation.

4. Experiments

Implementation Details: Our models are trained on a NVIDIA A5000 GPU with λ_{ssim} , λ_{GS} , and λ_{sD} set to 0.2, 0.5, and 0.1 respectively. The MLPs follow the Scaffold-GS framework [16]. View augmentation is applied every 3rd training iteration. The multi-view diffusion model is trained on the DL3DV-10K [14] dataset.

Table 2. Performance Metrics for Various Methods on Photo Tourism Dataset. The **best** and second-best results are highlighted.

Method	Brandenburg Gate		Sacre Coeur		Trevi Fountain	
	PSNR \uparrow	SSIM \uparrow	PSNR \uparrow	SSIM \uparrow	PSNR \uparrow	SSIM \uparrow
NeRF [18]	18.90	0.815	15.60	0.715	16.14	0.600
NeRF-W [17]	24.17	0.890	19.20	0.807	18.97	0.698
Ref-Fields [8]	26.64	0.886	22.26	0.817	23.42	0.737
3DGS [10]	19.37	0.880	17.44	0.835	17.58	0.709
GS-W [32]	23.51	0.897	19.39	0.825	20.06	0.723
SWAG [5]	26.33	0.929	21.16	<u>0.860</u>	23.10	0.815
WildGS [13]	<u>27.77</u>	<u>0.927</u>	<u>22.56</u>	0.859	23.63	0.766
Ours	28.69	0.929	23.76	0.861	<u>23.35</u>	<u>0.767</u>

Table 3. Results of several GS Methods on Nerf On-the-go Sets.

Method	Low Occlusion		Medium Occlusion		High Occlusion	
	PSNR \uparrow	SSIM \uparrow	PSNR \uparrow	SSIM \uparrow	PSNR \uparrow	SSIM \uparrow
3DGS [10]	19.68	0.649	19.19	0.709	19.03	0.649
GS-Opacity [31]	<u>20.54</u>	<u>0.662</u>	19.39	0.719	17.81	0.578
Mip-Splat [30]	20.15	0.661	19.12	0.719	18.10	0.664
GS-W [32]	18.67	0.595	21.50	0.783	18.52	0.644
WildGS [13]	20.62	0.658	22.80	<u>0.811</u>	23.03	<u>0.771</u>
Ours	19.85	0.777	<u>21.91</u>	0.822	<u>21.65</u>	0.832

Datasets: We conduct our experiments on four datasets. The Photo Tourism dataset features unconstrained user-uploaded images of popular monuments captured at different times and with varying camera models [21]. The NeRF On-the-go dataset includes casually captured indoor and outdoor sequences with varying occlusions [20]. We also evaluate on two WRIVA public data sets [1]—APL Image Density iPad (WRIVA-AIDI) and Massachusetts Task-Force Artifact (WRIVA-MTA)—which differ in image density and artifacts. Additionally, we test on two ULTRRA Development Sets [2], i.e., ImageDensity t01-v09-s00-r01 (ID-1901) and CameraModels t02-v06-s00-r01 (CM-2601).

4.1. Results Analysis

Tab. 1, Tab. 2 and Tab. 3 compares the proposed GS-Diff approach against several baselines and state-of-the-art methods. From Tab. 1, we observe that for a dense view set with good coverage in small area (e.g., ULTRRA ID-1901), all baselines perform comparably. However, in the WRIVA-AIDI experiments with sparse coverage, our method demonstrates a significant performance advantage. This highlights that integrating the diffusion prior and enhancing the base GS leads to notable performance improvements, particularly in sparse-view synthesis. For instance, in S06 set with 15 images, DreamSim drops from 0.34 for the base Scaffold-GS to 0.26 for our GS-only model, and further improves to 0.21 with the addition of diffusion prior. We also see significant improvement compared to the development baseline (i.e., Nerfacto) and vanilla 3DGS.

Experiments on the Photo Tourism dataset (Table 2) demonstrate that our approach performs comparably to the best prior methods in managing significant appearance vari-

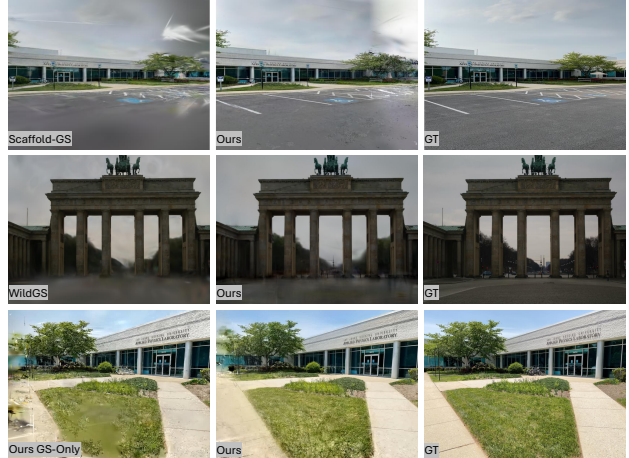


Figure 3. Comparison on the ULTRRA CM-2601 set (row-1), Photo Tourism Brandenburg Gate set (row-2), and WRIVA-AIDI 25 image set (row-3). Baselines (Left), Ours (Middle), GT (Right).

ations across inputs, while achieving overall better results than the state-of-the-art methods WildGS and SWAG. This highlights our method’s ability to preserve sharp details while effectively handling appearance changes. Similarly, on the ULTRRA CM-2601 dataset, which includes multiple camera models and appearance variations, our approach again outperforms the baselines.

Our experiments on the NeRF On-the-go dataset (Tab. 3) show that our model performs on par with prior methods in handling transient objects within scenes. However, since our approach assumes a fixed set of object classes for transients, it may struggle when an unknown object class appears as an occluder in the scene. Furthermore, results on the WRIVA-MTA sets in Table 1 show that our approach performs reasonably well in handling artifacts within the scene, despite not incorporating a dedicated artifact-handling mechanism in our GS framework.

Figure 3 presents three qualitative examples comparing our method to the baselines. It is clear that our approach produces less artifacts than the baseline methods (e.g., row-1 and row-3). Additionally, our method recovers finer details; for instance, in row-2, compared to WildGS, we observe improved textures in the bottom part of the image, which was heavily occluded in the training set.

5. Conclusions

Our proposed GS-Diff presents a novel 3D reconstruction framework that integrates the efficiency of 3D Gaussian Splatting with the generalization capabilities of multi-view diffusion models, while incorporating critical enhancements to tackle in-the-wild challenges. Experiments across multiple benchmark datasets demonstrate the high-quality performance of our method in addressing various challenges in unconstrained 3D reconstruction.

6. Acknowledgement

Supported by the Intelligence Advanced Research Projects Activity (IARPA) via Department of Interior/Interior Business Center (DOI/IBC) contract number 140D0423C0075. The U.S. Government is authorized to reproduce and distribute reprints for Governmental purposes notwithstanding any copyright annotation thereon. Disclaimer: The views and conclusions contained herein are those of the authors and should not be interpreted as necessarily representing the official policies or endorsements, either expressed or implied, of IARPA, DOI/IBC, or the U.S. Government.

References

- [1] Myron Brown, Michael Chan, and Michael Twardowski. Wriwa public data, 2024. [1](#), [4](#)
- [2] Neil Joshi; Joshua Carney; Nathanael Kuo; Homer Li; Cheng Peng; Myron Brown. Ultra challenge 2025, 2024. [1](#), [4](#)
- [3] David Charatan, Sizhe Lester Li, Andrea Tagliasacchi, and Vincent Sitzmann. pixelsplat: 3d gaussian splats from image pairs for scalable generalizable 3d reconstruction. In *Proceedings of the IEEE/CVF Conference on Computer Vision and Pattern Recognition*, pages 19457–19467, 2024. [1](#), [2](#)
- [4] Yuedong Chen, Haofei Xu, Chuanxia Zheng, Bohan Zhuang, Marc Pollefeys, Andreas Geiger, Tat-Jen Cham, and Jianfei Cai. Mvsplat: Efficient 3d gaussian splatting from sparse multi-view images. In *European Conference on Computer Vision*, pages 370–386. Springer, 2024. [2](#)
- [5] Hiba Dahmani, Moussab Bennehar, Nathan Piasco, Luis Roldao, and Dzmitry Tsishkov. Swag: Splatting in the wild images with appearance-conditioned gaussians. In *European Conference on Computer Vision*, pages 325–340. Springer, 2024. [2](#), [4](#)
- [6] Zhiwen Fan, Wenyan Cong, Kairun Wen, Kevin Wang, Jian Zhang, Xinghao Ding, Danfei Xu, Boris Ivanovic, Marco Pavone, Georgios Pavlakos, et al. InstantSplat: Unbounded sparse-view pose-free gaussian splatting in 40 seconds. *arXiv preprint arXiv:2403.20309*, 2(3):4, 2024. [2](#)
- [7] Ruiqi Gao, Aleksander Holynski, Philipp Henzler, Arthur Brussee, Ricardo Martin-Brualla, Pratul Srinivasan, Jonathan T Barron, and Ben Poole. Cat3d: Create anything in 3d with multi-view diffusion models. *arXiv preprint arXiv:2405.10314*, 2024. [2](#), [3](#)
- [8] Karim Kassab, Antoine Schnepf, Jean-Yves Franceschi, Laurent Caraffa, Jeremie Mary, and Valérie Gouet-Brunet. Refinedfields: Radiance fields refinement for unconstrained scenes. *arXiv preprint arXiv:2312.00639*, 2023. [4](#)
- [9] Bingxin Ke, Anton Obukhov, Shengyu Huang, Nando Metzger, Rodrigo Caye Daudt, and Konrad Schindler. Repurposing diffusion-based image generators for monocular depth estimation. In *Proceedings of the IEEE/CVF Conference on Computer Vision and Pattern Recognition*, pages 9492–9502, 2024. [3](#)
- [10] Bernhard Kerbl, Georgios Kopanas, Thomas Leimkühler, and George Drettakis. 3d gaussian splatting for real-time radiance field rendering. *ACM Trans. Graph.*, 42(4):139–1, 2023. [1](#), [2](#), [4](#)
- [11] Shakiba Kheradmand, Daniel Rebain, Gopal Sharma, Weiwei Sun, Jeff Tseng, Hossam Isack, Abhishek Kar, Andrea Tagliasacchi, and Kwang Moo Yi. 3d gaussian splatting as markov chain monte carlo. *arXiv preprint arXiv:2404.09591*, 2024. [2](#)
- [12] Xin Kong, Shikun Liu, Xiaoyang Lyu, Marwan Taher, Xiaojuan Qi, and Andrew J Davison. Eschernet: A generative model for scalable view synthesis. In *Proceedings of the IEEE/CVF Conference on Computer Vision and Pattern Recognition*, pages 9503–9513, 2024. [2](#), [3](#)
- [13] Jonas Kulhanek, Songyou Peng, Zuzana Kukelova, Marc Pollefeys, and Torsten Sattler. Wildgaussians: 3d gaussian splatting in the wild. *arXiv preprint arXiv:2407.08447*, 2024. [1](#), [2](#), [4](#)
- [14] Lu Ling, Yichen Sheng, Zhi Tu, Wentian Zhao, Cheng Xin, Kun Wan, Lantao Yu, Qianyu Guo, Zixun Yu, Yawen Lu, et al. D13dv-10k: A large-scale scene dataset for deep learning-based 3d vision. In *Proceedings of the IEEE/CVF Conference on Computer Vision and Pattern Recognition*, pages 22160–22169, 2024. [3](#)
- [15] Fangfu Liu, Wenqiang Sun, Hanyang Wang, Yikai Wang, Haowen Sun, Junliang Ye, Jun Zhang, and Yueqi Duan. Reconx: Reconstruct any scene from sparse views with video diffusion model. *arXiv preprint arXiv:2408.16767*, 2024. [2](#)
- [16] Tao Lu, Mulin Yu, Linning Xu, Yuanbo Xiangli, Limin Wang, Dahua Lin, and Bo Dai. Scaffold-gs: Structured 3d gaussians for view-adaptive rendering. In *Proceedings of the IEEE/CVF Conference on Computer Vision and Pattern Recognition*, pages 20654–20664, 2024. [2](#), [3](#)
- [17] Ricardo Martin-Brualla, Noha Radwan, Mehdi SM Sajjadi, Jonathan T Barron, Alexey Dosovitskiy, and Daniel Duckworth. Nerf in the wild: Neural radiance fields for unconstrained photo collections. In *Proceedings of the IEEE/CVF conference on computer vision and pattern recognition*, pages 7210–7219, 2021. [3](#), [4](#)
- [18] Ben Mildenhall, Pratul P Srinivasan, Matthew Tancik, Jonathan T Barron, Ravi Ramamoorthi, and Ren Ng. Nerf: Representing scenes as neural radiance fields for view synthesis. *Communications of the ACM*, 65(1):99–106, 2021. [1](#), [4](#)
- [19] Cheng Peng, Yutao Tang, Yifan Zhou, Nengyu Wang, Xijun Liu, Deming Li, and Rama Chellappa. Bags: Blur agnostic gaussian splatting through multi-scale kernel modeling. In *European Conference on Computer Vision*, pages 293–310. Springer, 2024. [2](#)
- [20] Weining Ren, Zihan Zhu, Boyang Sun, Jiaqi Chen, Marc Pollefeys, and Songyou Peng. Nerf on-the-go: Exploiting uncertainty for distractor-free nerfs in the wild. In *Proceedings of the IEEE/CVF Conference on Computer Vision and Pattern Recognition*, pages 8931–8940, 2024. [1](#), [4](#)
- [21] Noah Snavely, Steven M Seitz, and Richard Szeliski. Photo tourism: exploring photo collections in 3d. In *ACM siggraph 2006 papers*, pages 835–846. 2006. [1](#), [4](#)
- [22] Rundi Wu, Ben Mildenhall, Philipp Henzler, Keunhong Park, Ruiqi Gao, Daniel Watson, Pratul P Srinivasan, Dor

- Verbin, Jonathan T Barron, Ben Poole, et al. Reconfusion: 3d reconstruction with diffusion priors. In *Proceedings of the IEEE/CVF Conference on Computer Vision and Pattern Recognition*, pages 21551–21561, 2024. 2, 3
- [23] Tianyi Xie, Zeshun Zong, Yuxing Qiu, Xuan Li, Yutao Feng, Yin Yang, and Chenfanfu Jiang. Physgaussian: Physics-integrated 3d gaussians for generative dynamics. In *Proceedings of the IEEE/CVF Conference on Computer Vision and Pattern Recognition*, pages 4389–4398, 2024. 3
- [24] Haolin Xiong, Sairisheek Muttukuru, Rishi Upadhyay, Pradyumna Chari, and Achuta Kadambi. Sparsegs: Real-time 360 $\{\backslash\text{deg}\}$ sparse view synthesis using gaussian splatting. *arXiv preprint arXiv:2312.00206*, 2023. 1, 2, 3
- [25] Haofei Xu, Songyou Peng, Fangjinhua Wang, Hermann Blum, Daniel Barath, Andreas Geiger, and Marc Pollefeys. Depthspat: Connecting gaussian splatting and depth. *arXiv preprint arXiv:2410.13862*, 2024. 2
- [26] Jiacong Xu, Yiqun Mei, and Vishal M Patel. Wild-gs: Real-time novel view synthesis from unconstrained photo collections. *arXiv preprint arXiv:2406.10373*, 2024. 2
- [27] Ziyi Yang, Xinyu Gao, Yangtian Sun, Yihua Huang, Xiaoyang Lyu, Wen Zhou, Shaohui Jiao, Xiaojuan Qi, and Xiaogang Jin. Spec-gaussian: Anisotropic view-dependent appearance for 3d gaussian splatting. *arXiv preprint arXiv:2402.15870*, 2024. 2
- [28] Zongxin Ye, Wenyu Li, Sidun Liu, Peng Qiao, and Yong Dou. Absgs: Recovering fine details in 3d gaussian splatting. In *Proceedings of the 32nd ACM International Conference on Multimedia*, pages 1053–1061, 2024. 2, 3
- [29] Wangbo Yu, Jinbo Xing, Li Yuan, Wenbo Hu, Xiaoyu Li, Zhipeng Huang, Xiangjun Gao, Tien-Tsin Wong, Ying Shan, and Yonghong Tian. Viewcrafter: Taming video diffusion models for high-fidelity novel view synthesis. *arXiv preprint arXiv:2409.02048*, 2024. 2
- [30] Zehao Yu, Anpei Chen, Binbin Huang, Torsten Sattler, and Andreas Geiger. Mip-splatting: Alias-free 3d gaussian splatting. In *Proceedings of the IEEE/CVF Conference on Computer Vision and Pattern Recognition*, pages 19447–19456, 2024. 2, 3, 4
- [31] Zehao Yu, Torsten Sattler, and Andreas Geiger. Gaussian opacity fields: Efficient and compact surface reconstruction in unbounded scenes. *arXiv preprint arXiv:2404.10772*, 2024. 2, 3, 4
- [32] Dongbin Zhang, Chuming Wang, Weitao Wang, Peihao Li, Minghan Qin, and Haoqian Wang. Gaussian in the wild: 3d gaussian splatting for unconstrained image collections. In *European Conference on Computer Vision*, pages 341–359. Springer, 2024. 4
- [33] Richard Zhang, Phillip Isola, Alexei A Efros, Eli Shechtman, and Oliver Wang. The unreasonable effectiveness of deep features as a perceptual metric. In *Proceedings of the IEEE conference on computer vision and pattern recognition*, pages 586–595, 2018. 3
- [34] Zehao Zhu, Zhiwen Fan, Yifan Jiang, and Zhangyang Wang. Fsgs: Real-time few-shot view synthesis using gaussian splatting. In *European Conference on Computer Vision*, pages 145–163. Springer, 2024. 2
- [35] Matthias Zwicker, Hanspeter Pfister, Jeroen Van Baar, and Markus Gross. Ewa volume splatting. In *Proceedings Visualization, 2001. VIS'01.*, pages 29–538. IEEE, 2001. 2